Theoretical interpretation of the systematics of effective single-particle level densities from (n,p) reactions at 14.8 MeV energy

H. S. Hans, Gulzar Singh, A. Kumar,* K. P. Singh, and B. R. Behera
Department of Physics, Panjab University, Chandigarh, India

Sudip Ghosh
Saha Institute of Nuclear Physics, Calcutta, India

(Received 16 August 2011; published 14 May 2012)

The universal experimental data for the energy-integrated angular distribution and the angle-integrated energy spectra for protons emitted from the (n,p) reactions at 14.8 MeV incident energy were analyzed earlier using the computer code PRECO-D2, developed on the basis of Kalbach's semiempirical model for the preequilibrium reactions. The results of the analysis provided the semiempirical systematics of the single-particle level densities $g_R(\text{exp})$ (effective in the residual nuclei) and $g_c(\text{exp})$ (effective in the composite system). In order to interpret these results, we have carried out the theoretical calculations with Shlomo's theory developed on the basis of the Green's function approach. The theoretical values based on Shlomo's theory for $g_{Rn}^{Th}(\varepsilon_{Rn})$ and $g_{Rp}^{Th}(\varepsilon_{Rp})$ for the residual nucleus and $g_{cn}^{Th}(\varepsilon_{cn})$ and $g_{cp}^{Th}(\varepsilon_{cp})$ for the composite systems, respectively, were calculated at various excitation energies by using a reasonable single-particle nuclear potential strength V_0, available from systematics in literature. Here, ε_{Rn} and ε_{Rp} are the single-particle excitation energies for single-particle level densities for the residual nucleus, and ε_{cn} and ε_{cp} are the single-particle excitation energies of effective single-particle level densities for the composite system for neutrons and protons, respectively. The Coulomb interaction potential V_c was included for protons over and above the nuclear potential V_0. The total theoretical values were taken as $g_R^{TTh}(\varepsilon_R) = g_{Rn}^{Th}(\varepsilon_{Rn}) + g_{Rp}^{Th}(\varepsilon_{Rp})$ for residual nuclei and $g_c^{TTh}(\varepsilon_c) = g_{cn}^{Th}(\varepsilon_{cn}) + g_{cp}^{TTh}(\varepsilon_{cp})$ for the composite system. ε_R is the Fermi energy of the total effective single-particle level density for residual nuclei, and ε_c is the excitation energy of the effective single-particle level density of the composite system. Careful comparison of theoretical and experimental results shows that $g_R(\text{exp})$ matches with $g_R^{TTh}(\varepsilon_f)$ for $V_0^i = 45$ MeV where (ε_f) is the Fermi energy. The theoretical values $g_R^{TTh}(\varepsilon_f)$ also nearly agree with the previously reported values by various groups, obtained through different approaches for a large number of cases. The values of $g_c(\text{exp})$ always are found to be greater than $g_R(\text{exp})$ and match with $g_c^{TTh}(\varepsilon_c)$ at effective excitation energies ε_c, which are found to be invariably much higher than the respective ε_f and are positive and follow the nuclear shell model structure when plotted against A. This supports the concept that the values of effective $g_c(\text{exp})$ are decided mainly by dominant transition, which occurs during initial stages of the multistep statistical direct preequilibrium process that involves unbound states. The values of $g_R(\text{exp})$, on the other hand, are found to correspond to the effective ε_R around the Fermi energies of the bound states of residual nuclei involved in the decay processes. The ratios of $g_c(\text{exp})/g_R(\text{exp})$ are found to follow the $(\frac{\langle\varepsilon_c\rangle}{\langle\varepsilon_f\rangle})^{1/2} f$ description and to match Shlomo's theory.

DOI: 10.1103/PhysRevC.85.054614 PACS number(s): 21.10.Ma, 24.60.Dr, 24.60.Gv, 25.40.Kv

I. INTRODUCTION

In an earlier paper [1], the authors analyzed the universal experimental data on protons emitted in (n,p) reactions at 14.8 MeV nominal neutron energy, the angle-integrated energy spectra and the energy-integrated angular distributions (EIAD) of protons for $E \geqslant 3$ MeV (EIAD) on the basis of the Kalbach model of preequilibrium, which used the PRECO-D2 computer code [1,2]. Apart from other information, it yielded the semiempirical values for the effective single-particle level densities $g_R(\text{exp})$ for the bound states for residual nuclei and for $g_c(\text{exp})$ for the composite system, which participate in the initial dominant stages of the preequilibrium process. The PRECO-D2 computer code fitted the exact shapes of the energy spectra, especially at the high-energy side and the shapes of angular distribution especially in the forward direction, by varying the values of $g_R(\text{exp})$ and $g_c(\text{exp})$, which were fed into the PRECO-D2 computer program by using a trial-and-error procedure.

After our data were published in Ref. [1], Shlomo and co-workers [3–6] derived expressions for single-particle level densities on the basis of the Green's-function approach under the Thomas-Fermi (TF) approximation by using finite and infinite single-particle potential wells. They derived closed expressions for $g^{\text{TF}}(\epsilon)$, the semiclassical Thomas-Fermi single-particle level densities, for the trapezoidal (TR) finite potential for nuclear reactions. Also, expressions for $g(\text{free})$ were derived for the correction due to free single-particle level densities for $\epsilon > 0$. The values of effective single-particle level densities $g(\epsilon)$ then, can be calculated for excitation energy ϵ, specified with respect to zero energy as

$$g(\epsilon) = g^{\text{TF}}(\epsilon) - g_{\text{free}}(\epsilon). \quad (1)$$

In the present paper, we have compared our semiempirical values of $g_R(\text{exp})$ and $g_c(\text{exp})$, for cases with gross variations with A as derived in Ref. [1], with the theoretically expected

*ashok@pu.ac.in

values from Shlomo's theory in order to develop excitation energy systematics for g_R(exp) and g_c(exp).

Below, we give the perspective of the Kalbach model as applied in the analysis of experimental data while extracting the values of g_R(exp), g_c(exp), and the Shlomo model as used for the calculation of the excitation energies of single-particle level densities.

II. THEORETICAL CONSIDERATIONS

A. Kalbach model

The logic of the Kalbach model as used in the computer PRECO-D2 program is based intrinsically on the quantum-mechanical treatment of the preequilibrium statistical processes as used by Feshbach *et al*. [7]. They divided the reaction cross section into two parts: the first part, which exhibits forward-peaked angular distributions and high-energy-peaked energy spectra as due to preequilibrium-based multistep statistical direct (MSD) processes, and the second part as the symmetric angular distributions term and low-energy-peaked energy spectra as the multistep statistical compound (MSC) processes. The quantum-mechanical treatment basically is based on the exciton model of Griffin [8].

The preequilibrium process represents a continuum of a few step processes (through $\bar{n}$ steps) between direct and compound nuclei to form a composite nucleus at excitation energy ε_c from the base state of the nucleus, which decays through light-particle evaporation to the residual nucleus at excitation energy ε_R.

In nuclear reactions with neutrons at an incident energy of 14.8 MeV, the preequilibrium processes become important where the entrance channel undergoes only one- and two-body residual interactions for $En \geqslant 10$ MeV. In the exciton model [8–10], a cascade of residual two-body interactions takes the projectile target composite nucleus from the initial single state specified by the exciton number ($n_0 = p_0 + h_0$) through progressively more complex configurations to the final compound nucleus equilibrium states ($\bar{n} = \bar{p} + \bar{h}$). Each stage of the binary state is specified by the number p of the particles excited and the number h of the holes.

In the early stages of the cascade [11–14], the particle-hole creation constitutes the dominant binary residual interaction, and if the excitation energy of the intermediate nucleus is large enough, it results in unbound states for particle emission. The preequilibrium emission can take place from any of these unbound states at excitation energies ε_c through MSD processes, which dominate for unbound states for $\hbar \leqslant 2$ by leaving the residual nucleus at excitation energies of ε_R.

In later stages of the cascade, the states grow in complexity, and some of the states may be bound. Particle-hole annihilation and scattering due to residual interaction and the statistical fluctuations may change some bound states to unbound states, which results in preequilibrium emission through the MSC process.

The cross sections of the energy spectra of the preequilibrium ejectiles can be expressed [15] as

$$\sigma_{\mathrm{PRE}}(E) = \sigma_{\mathrm{MSD}}(E) + \sigma_{\mathrm{MSC}}(E), \tag{2}$$

where $\sigma_{\mathrm{PRE}}(E)$ and $\sigma_{\mathrm{MSD}}(E)$ are calculated from the following expressions:

$$\sigma_{\mathrm{PRE}}(E) = \sigma_{\mathrm{ABS}} \sum_{n=p_0}^{\bar{p}} S_U(p,h) T_U(p,h) \lambda_c^U(p,h,E), \tag{3a}$$

and

$$\sigma_{\mathrm{MSD}}(E) = \sigma_{\mathrm{ABS}} \sum_{n=p_0}^{\bar{p}} S_d(p,h) T_U(p,h) \lambda_c^U(p,h,E), \tag{3b}$$

so that

$$\sigma_{\mathrm{MSC}} = \sigma_{\mathrm{PRE}}(E) - \sigma_{\mathrm{MSD}}. \tag{4}$$

Here, σ_{ABS} is the absorption cross reaction of the projectile on the target. The symbol p_0 stands for the number of particles excited for the first stage of the binary cascade, and $\bar{p}$ is the number of particles excited in the most probable states at equilibrium. $S_U(p,h)$ denotes the probability of reaching an unbound configuration with p excited particles and h holes from either bound or unbound previous states. However, $S_d(p,h)$ is confined to that (p,h) configuration that has evolved through only unbound configurations and leads to the MSD process. $T_U(p,h)$ is the mean life of the (p,h) configuration, and $\lambda_c^U(p,h,E)$ is the emission rate of the ejectile. Then, $\sigma_{\mathrm{PRE}}(E)$ and $\sigma_{\mathrm{MSD}}(E)$ are evaluated from Eqs. (2) and (3b), and σ_{MSC} is obtained from Eqs. (4), (3a), and (3b). Then,

$$\sigma_{\mathrm{Comp}} = \sigma_{ev} + \sigma_{\mathrm{MSC}}, \tag{5}$$

where σ_{ev} for evaporation is obtained from the Weisskopf-Ewing evaporation model calculations [15].

As described by Kalbach [16], the above relationships are included in the computer program PRECO-D, which is based on a modification of their code PRECO-B, developed in 1977 and 1978 [13,16]. In PRECO-D, the contribution due to the MSD and MSC reaction mechanisms also were calculated separately as shown above.

The calculation of $\lambda^U(p,h,E)$ in Eqs. (3a) and (3b) involves particle state densities $\rho(p,h,E)$ of the simple (of a few quasiparticle) bound and unbound states in the composite system and the particle density of simple bound states in the residual nucleus. The expression for particle state densities of simple unbound and bound states involves the values of effective single-particle level densities in the composite system and residual nuclei.

However, in Ref. [1], we have used the computer code PRECO-D2 in which a provision is made to choose the effective single-particle level densities g_1, g_2, g_3, and g_4 by a trial-and-error method to fit the experimental data where $g_1 = g_c$(exp) corresponds to the composite system and $g_2 = g_3 = g_4 = g_R$(exp) belong to the residual nuclei for preequilibrium particle decay processes. We have used the same g_R(exp) for the residual nuclei for protons, neutrons, and α decay of composite systems. We have adjusted g_c(exp) and g_R(exp) by the trial-and-error method to reproduce the experimental data of the energy spectrum of protons corresponding to the high-energy end and the angular distribution in the forward direction in the (n, p) reaction at 14.8 MeV incident energy as shown in Ref. [1].

TABLE I. The experimental values of g_c(exp) and g_R(exp) from composite and residual nuclei from the (n,p) reaction at an incident energy of 14.8 MeV extracted by using the Kalbach model [1,2].

Number	Target	g_c(exp)	g_R(exp)
1	^{19}F	2.49	1.52
2	^{24}Mg	2.78	2.01
3	^{27}Al	2.87	2.37
4	^{28}Si	2.49	1.52
5	^{31}P	2.80	2.49
6	^{32}S	2.49	2.43
7	^{40}Ca	4.50	2.98
8	^{47}Ti	4.50	2.01
9	^{48}Ti	4.07	2.01
10	^{50}Ti	4.07	2.98
11	^{56}Fe	5.47	4.01
12	^{59}Co	4.99	4.01
13	^{58}Ni	6.02	4.50
14	^{65}Cu	5.47	2.98
15	^{64}Zn	4.99	2.98
16	^{66}Zn	5.47	4.01
17	^{89}Y	9.00	6.54
18	^{103}Rh	10.30	7.54
19	^{106}Pd	11.00	7.55
20	^{108}Pd	10.40	7.54
21	^{107}Ag	10.09	7.93
22	^{109}Ag	10.52	7.56
23	^{115}In	11.00	7.93

Many attempts of the trial-and-error procedure finally reproduced the experimental data, which yield the correct values of g_R(exp) and g_c(exp). We have given these values in Table I, reproduced from Ref. [1].

B. Shlomo's theory

According to Shlomo and co-workers [3–6], one calculates the exact values of the single-particle level densities $g_B(\epsilon)$ for bound and continuous states using a Green's-function [6,17,21] approach with the Strutinski smoothing [17] procedure. They have considered, in particular, the methods of TF [18,19] approximation. By taking the single-particle Hamiltonian H as

$$H = p^2/2m + V(r), \tag{6}$$

for the bound states, they have written

$$g_B(\epsilon) = \sum_i \delta(\epsilon - \epsilon_i), \tag{7}$$

where energies ϵ_i of the bound states are given by

$$H\Psi_i = \epsilon_i \Psi_i, \tag{8}$$

and for the finite well, the continuum contributions are determined [6] from the scattering phase shifts. By writing the single-particle level density in terms of the Green's [20] function $G(\bar{r}, \bar{r}, \epsilon + ia)$ as

$$g(\epsilon) = \frac{1}{2\pi} \int d^3r [(G(\vec{r}, \vec{r}\epsilon + ix))]_{\vec{r}=\vec{r}} = \sum_n \delta(\epsilon_n - \epsilon), \tag{9}$$

and by following the above procedure, the level densities of the single-particle states were calculated earlier [20,21] in the framework of the TF approximation as

$$g_{\rm TF}(\epsilon) = \left(\frac{2m}{\hbar^2}\right)^{3/2} \frac{Dg}{4\pi^2} \int (\epsilon - V)^{1/2} \Theta(\epsilon - V) dr^3, \tag{10}$$

where Dg is the degeneracy of the single-particle levels and

$$\Theta(X) = \begin{cases} 1, & x \geqslant 0, \\ 0, & x \leqslant 0. \end{cases} \tag{11}$$

Shlomo [3] used only the volume part of the expression and obtained

$$g_{\rm TF}(\epsilon) = \left(\frac{2m}{\hbar^2}\right)^{3/2} \frac{1}{2\pi^2} \int d^3r (E - V)^{1/2} \Theta(\epsilon - V). \tag{12}$$

According to Bogila *et al.* [4], the trapezoidal finite potential for nuclear interaction is given by

$$V(r) = \begin{cases} V_0 & \text{for } r < R - D, \\ 1/2\,[1 - (r-R)/D]\,V_0 & \text{for } R - D < r < R + D \end{cases} \tag{13}$$

for which the expression for $g^{\rm TF}(\epsilon)$ is given by

$$g_{\rm TF}(\epsilon) = 1/2\pi^2 (2m/\hbar^2)^{3/2} \frac{[4\pi(R-D)^3]}{3} \times (\epsilon - V_0)^{1/2} [1 + 2x + (8/15)x^2 + (16/35)x^3], \tag{14}$$

where $x = -[2D(\epsilon - V_0)]/[(R - D)V_0)]$. Here, the excitation energy ϵ is measured from the ground-state energy, which is zero. According to the authors, for the case of $\epsilon > 0$, the corresponding semiclassical expression $g_{\rm TF}(\epsilon)$ for the finite-depth trapezoidal potential well should be corrected by subtracting the contribution due to the free level density $g_{\rm free}(\epsilon)$ for obtaining the single-particle level density $g(\epsilon)$. The expression for $g_{\rm free}(\epsilon)$ is given by [3,4]

$$g_{\rm free}(\epsilon) = 1/2\pi^2 (2m/\hbar^2)^{3/2} \frac{[4\pi(R+D)^3]}{3} \times \epsilon^{1/2} [1 + 2y + (8/15)y^2 + (16/35)y^3], \tag{15}$$

with

$$y = -2D\epsilon/[(R + D)V_0]. \tag{16}$$

Furthermore, the following parameters were used for the single-particle potential well:

$$V_0 = -V_0^i + 33t_3(N - Z)/A(\text{MeV}), \quad D = \pi d \quad (d = 0.7\ \text{fm}), \tag{17}$$

$$R = R_0 \Big/ \left[1 + \left(\frac{D}{R}\right)^2\right]^{1/3}, \quad R_0 = 1.12A^{1/3} + 1.0(\text{fm}), \quad V_0^i = 40, 45, 50, \quad \text{or} \quad 54\,\text{MeV}, \tag{18}$$

where N and Z are the number of neutrons and protons, $t_3 = 1$ for neutrons and -1 for protons. The value of R is determined by the iteration method.

The potential $V(r)$, as given in Eq. (13) with V_0 given in Eqs. (17) and (18), corresponds to a pure nuclear interaction,

which, if used in Eqs. (13)–(16), corresponds to the excitation of neutrons. For the excitation of protons, we will have to take the Coulomb potential $V_c(r)$ into account over and above the nuclear potential $V_n(r)$. Then, one may write [3]

$$V(r) = V_n(r) + V_c(r), \tag{19}$$

where

$$V_c(r) = [Ze^2/2R_c](3 - (r/R_c)^2 \quad r \leqslant R_c$$
$$= \frac{Ze^2}{r} \quad r \geqslant R_c \tag{20}$$

whereas, $V_n(r)$ is given by Eqs. (13) and (17).

The closed expression for the value of the single-particle level density with Coulomb interaction is not available in literature with the values of $V(r)$ as given in Eqs. (19) and (20). However, we have used an approximation where we have replaced the value of V_0 in Eqs. (13)–(17) by

$$V_0 + V_c, \quad \text{where} \quad V_c = Ze^2/R_c, \tag{21}$$

so that V_c is taken as the Coulomb potential at radius R_c. We have used $R_c = R$. As the value of V_0 is negative, whereas, the value of V_c is positive, it reduces the effective value of $V(r)$ in Eq. (13). Then, $g_c^{TTh}(\epsilon) = g^{\mathrm{TF}}(\epsilon) - g_{\mathrm{free}}(\epsilon)$.

Below, we describe the results of our comparison of the experimental values with those calculated on the basis of Shlomo's theory:

(i) For energies ε_R of the residual nuclei and
(ii) for composite excited states at excitation energies ε_c.

III. ANALYSIS OF DATA: CALCULATIONS

A. For residual nuclei

We have calculated the values of single-particle level densities $g_{Rn}^{Th}(\epsilon_{Rn})$ for neutron excitation by using the expression for $g_{Rn}^{\mathrm{TF}}(\epsilon_{Rn})$ in Eq. (14) and by obtaining the relation $(\epsilon_n - V_0)^{1/2} = [|V_0| - (B_E)_n]^{1/2}$, where V_0 is taken from Eq. (17) with $V_0^i = 40, 45, 50, 54$ MeV, $t_3 = 1$, and $(B_E)_n$ is the binding energy of neutrons. The value of g_n(free) is taken to be zero.

Similarly, for proton excitation, we have used the relation $(\epsilon_p - V_0)^{1/2} = [|V_0| - (B_E)_p - |V_c|]^{1/2}$ in the expression for $g_{Rp}^{Th}(\varepsilon_{Rp})$ in Eq. (14) where $(B_E)_p$ is the binding energy of protons. Of course, V_c is the Coulomb potential as given in Eq. (21). Also, in other parts of the expression, we have replaced $|V_0|$ by $|V_0| - |V_c|$ in the expression where V_0 is taken to be $t_3 = -1$. Also, g_p(free), again, is taken to be zero.

We finally express the relation,

$$g_R^{TTh}(\varepsilon_R) = g_{Rn}^{Th}(\varepsilon_{Rn}) + g_{Rp}^{Th}(\varepsilon_{Rp}), \tag{22}$$

where

$$\varepsilon_{Rn} = (|V_0| - |(B_E)_n|) = \varepsilon_{nf},$$

and

$$\varepsilon_{Rp} = (|V_0| - |(B_E)_p|) - |V_c| = \varepsilon_{pf},$$

and ε_R is the excitation energy of the total effective single-particle level density around the effective Fermi energy ε_f of the residual nucleus, expressed as $\varepsilon_f = (\varepsilon_{nf} + \varepsilon_{pf})/2$. The values of $g_{Rn}^{Th}(\varepsilon_{nf})$ for neutrons, $g_{Rp}^{Th}(\varepsilon_{pf})$ for protons, total value $g_R^{TTh}(\varepsilon_f)$, and the values of the Fermi energy ε_f are

TABLE II. The theoretical values of single-particle level densities for excitation for neutrons $g_{Rn}^{Th}(\varepsilon_{nf})$, for protons $g_{Rp}^{Th}(\varepsilon_{pf})$, and for the total $g_R^{TTh}(\varepsilon_f) = g_{Rn}^{Th}(\varepsilon_{nf}) + g_{Rp}^{Th}(\varepsilon_{pf})$, based on Shlomo's model where ε_{pf} is the Fermi energy for the proton, ε_{nf} is the Fermi energy for the neutron, and ε_f is the average Fermi energy, i.e., $\varepsilon_f = \frac{\varepsilon_{pf}+\varepsilon_{nf}}{2}$.

Z	A	$g_{Rn}^{Th}(\varepsilon_{nf})$	$g_{Rp}^{Th}(\varepsilon_{pf})$	$g_R^{TTh}(\varepsilon_f)$	ε_f (MeV)
			(a)		
$V_0^i = 40$ MeV					
9	19	0.79	0.80	1.59	29.54
12	24	0.96	0.83	1.78	27.96
13	27	1.00	0.97	1.97	29.02
14	28	1.01	0.86	1.86	27.05
15	31	1.12	1.07	2.20	29.14
16	32	1.13	0.99	2.13	28.18
20	40	1.41	1.20	2.61	28.14
22	44	1.49	1.28	2.76	28.22
22	47	1.58	1.49	3.07	26.99
22	50	1.79	1.71	3.49	27.28
26	56	1.90	1.72	3.62	27.23
27	59	1.99	1.90	3.89	28.32
28	58	1.85	1.62	3.47	27.25
29	65	2.26	2.21	4.47	28.78
30	64	2.13	1.95	4.08	28.10
30	66	2.26	2.11	4.38	28.02
39	89	2.92	2.82	5.74	27.97
45	103	3.34	3.19	6.53	27.86
46	106	3.59	3.32	6.91	26.76
46	108	3.49	3.19	6.69	26.81
47	107	3.41	3.25	6.66	27.77
47	109	3.51	3.37	6.88	27.66
49	115	3.66	3.53	7.19	27.36
$V_0^i = 45$ MeV					
9	19	0.90	0.91	1.81	34.54
12	24	1.08	0.96	2.04	32.96
13	27	1.14	1.11	2.26	34.02
14	28	1.15	1.01	2.16	32.05
15	31	1.28	1.23	2.51	34.14
16	32	1.29	1.16	2.45	33.18
20	40	1.60	1.40	3.00	33.14
22	47	1.69	1.49	3.18	33.22
22	48	1.80	1.71	3.51	31.99
22	50	2.01	1.94	3.95	32.28
26	56	2.15	1.97	4.13	32.23
27	59	2.25	2.17	4.41	33.32
28	58	2.11	1.89	3.99	32.25
29	65	2.54	2.49	5.03	33.78
30	64	2.40	2.24	4.64	33.10
30	66	2.55	2.40	4.95	33.02
39	89	3.28	3.19	6.48	32.97
45	103	3.75	3.61	7.36	32.86
46	106	4.02	3.76	7.78	31.76
46	108	3.91	3.63	7.54	31.81
47	107	3.84	3.68	7.52	32.77
47	109	3.94	3.81	7.75	32.66
49	115	4.11	3.99	8.10	32.36

TABLE II. (*Continued.*)

Z	A	$g_{Rn}^{Th}(\varepsilon_{nf})$	$g_{Rp}^{Th}(\varepsilon_{pf})$	$g_R^{TTh}(\varepsilon_f)$	ε_f (MeV)
			(b)		
$V_0^i = 50$ MeV					
9	19	1.01	1.01	2.02	39.54
12	24	1.20	1.08	2.29	37.96
13	27	1.28	1.24	2.52	39.02
14	28	1.29	1.15	2.44	37.05
15	31	1.43	1.38	2.81	39.14
16	32	1.44	1.32	2.76	38.18
20	40	1.77	1.59	3.36	38.14
22	47	1.88	1.70	3.57	38.22
22	48	2.01	1.92	3.93	36.99
22	50	2.23	2.15	4.38	37.28
26	56	2.38	2.21	4.60	37.23
27	59	2.49	2.41	4.90	38.32
28	58	2.35	2.14	4.48	37.25
29	65	2.80	2.75	5.55	38.78
30	64	2.66	2.50	5.16	38.10
30	66	2.81	2.67	5.48	38.02
39	89	3.62	3.53	7.16	37.97
45	103	4.13	4.00	8.13	37.86
46	106	4.41	4.17	8.58	36.76
46	108	4.30	4.03	8.33	36.81
47	107	4.23	4.09	8.32	37.77
47	109	4.34	4.22	8.56	37.66
49	115	4.53	4.42	8.95	37.36
$V_0^i = 54$ MeV					
9	19	1.08	1.09	2.17	43.54
12	24	1.29	1.18	2.47	41.96
13	27	1.38	1.35	2.72	43.08
14	28	1.39	1.25	2.64	41.05
15	31	1.54	1.49	3.03	43.14
16	32	1.55	1.43	2.99	42.18
20	40	1.90	1.73	3.63	42.14
22	47	2.02	1.85	3.87	42.22
22	48	2.16	2.08	4.25	40.99
22	50	2.39	2.31	4.70	41.28
26	56	2.56	2.39	4.95	41.23
27	59	2.67	2.60	5.27	42.32
28	58	2.53	2.33	4.85	41.25
29	65	3.00	2.95	5.94	42.78
30	64	2.85	2.71	5.56	42.10
30	66	3.01	2.88	5.89	42.02
39	89	3.88	3.79	7.67	41.97
45	103	4.42	4.30	8.71	41.86
46	106	4.71	4.47	9.18	40.76
46	108	4.59	4.34	8.93	40.81
47	107	4.53	4.39	8.92	41.77
47	109	4.64	4.53	9.17	41.66
49	115	4.85	4.74	9.59	41.36

given in Table II for $V_0^i = 40$, 45, 50, and 54 MeV for various targets.

We found, by comparison with g_R(exp), that the values of $g_R^{TTh}(\varepsilon_R)$ that correspond to $V_0^i = 45$ MeV matched well with g_R(exp) as shown in Fig. 1. From Fig. 1, it is quite evident that theoretical values of single-particle level densities for $V_0^i =$

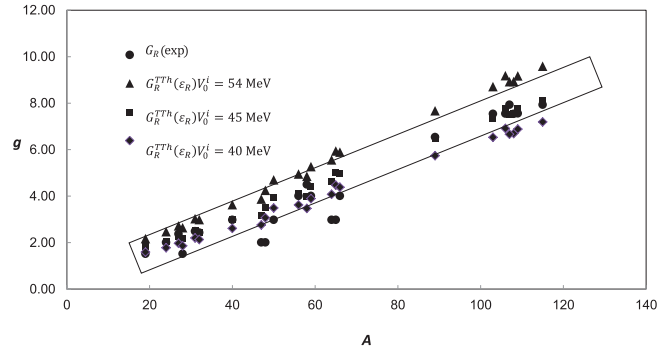

FIG. 1. (Color online) The values of $g_R^{TTh}(\varepsilon_f)$ at $V_0^i = 54$, 45, and 40 MeV and the value of g_R(exp) as a function of mass number A (Table I and Table II).

54 MeV are higher and theoretical values for $V_0^i = 40$ MeV are lower than the values of g_R(exp). We, therefore, conclude that ε_R calculated by using $V_0^i = 45$ MeV in Eq. (17) corresponds to the Fermi energy for incident neutrons at 14.8 MeV if we take both neutron excitation as well as proton excitation into account.

The values of compound nuclear level density parameter a are related to the single-particle level density g at the Fermi energy by

$$a = \frac{\pi^2}{6} g.$$

The values of a have been calculated by Behkami *et al.* [22] for a large number of nuclei ($A = 20$ to $A = 250$) by using the Bethe formula and the BCS model. Also, Al-Quraishi *et al.* [23] have calculated the values of a on the basis of two formulas (i) $a = \propto A$ and (ii) $a = \propto A/\exp[\beta(N-Z)^2]$ over a wide range of A (from $A = 24$ to $A = 200$). Also, in the same year, Bency John *et al.* [24] measured α emission spectra from a number of heavy-ion-induced reactions, which populate compound nuclei in the range of $A = 108$–208. The data were analyzed by a statistical model code, which yielded $K = \frac{A}{a}$ where a is the same nuclear level density parameter as described above.

We have given these values of g, obtained from the above calculations, in Table III and have plotted them in Fig. 2. We also have compared these values of g from literature with $g_R^{TTh}(\varepsilon_f)$ obtained from Shlomo's model with $V_0^i = 45$ MeV. These seem to nearly match.

We, therefore, conclude that Shlomo's model with $V_0^i = 45$ MeV explains both the experimental values of g_R(exp), effective for residual nuclei derived from the Kalbach model, and the values of single-particle level density at the Fermi energy ε_f as reported earlier by many other authors of the compound nuclei process. Also, the excitation energy of the single-particle level densities g_R(exp) of the residual nuclei derived from the Kalbach model for preequilibrium processes is close to the Fermi energy.

B. For the composite state

To calculate the single-particle level density for the composite nuclear system at high excitation energies ε_c, we use

TABLE III. The semiempirical values of $g(\epsilon_f)$ as calculated by Behkami *et al*. on the basis of the BCS model (g_s) and Bethe's model (g_B) and by Al-Quraishi *et al*. and Bency John *et al*. for various targets along with theoretical values of single-particle level densities $g_R^{TTh}(\varepsilon_f)$ at the Fermi energy based on the Shlomo model for $V_0^i = 45$ MeV.

Serial no.	A	$g_R^{TTh}(\varepsilon_f)$	Behkami *et al*. [22]			A	Al-Quraishi *et al*. [23]	Bency John *et al*. [24]
		$V_0^i = 45$ MeV	A	g_B	g_S			
1	19	1.81	20	1.50	2.40	24	1.60	
2	24	2.04	22	1.00	1.70			
3	27	2.26	24	1.00	1.80	28	1.87	
4	28	2.16	24	2.60	1.80			
5	31	2.51	25	1.50	1.60			
6	32	2.45	26	1.30	1.80			
7	40	3.00	28	1.80	2.00	40	2.67	
8	47	3.18	28	1.80	2.00			
9	48	3.51	28	2.60	2.10			
10	50	3.95	29	2.90	2.10			
11	56	4.13	30	1.50	2.20	56	3.73	
12	58	3.99	31	2.00	2.40			
13	59	4.41	34	2.10	2.60			
14	64	4.64	40	2.20	3.10			
15	65	5.03	41	2.90	3.20			
16	66	4.95	55	3.10	4.10	70	4.67	
17	89	6.48	60	4.10	4.50			
18	103	7.36	61	3.60	4.60	100	6.69	
19	106	7.54	67	4.70	3.90		6.81	
20	107	7.52	106	7.80	8.10			
21	108	7.78	109	7.90	8.40			
22	109	7.75	116	9.00	8.50	108	8.19	8.46
23	115	8.10						
24	108	7.78		8.20	8.23			
25	122	8.02		8.85	9.20	122	8.19	8.46
26	128	8.36		8.31	9.66			
27	134	8.71	134	7.80	10.06	134		10.30
28	151	9.53	151	11.54	11.51	151	6.69	
29	168	10.36	168	10.23	12.29			11.48
30	172	10.70	172	10.70	13.24	171		13.5
31	178	11.00	178	11.14	12.50	172		12.96
32	190	11.58	190	11.41	13.59	173		11.4
33	198	12.39	198	9.29	13.58	177		13.4
34	200	12.22	200	8.10	13.86	180		13.6
35	207	12.69	207	5.80	12.31	188		14.2
36	231		231	15.92	12.84	200	13.38	
37	240	14.51	240	14.09	13.62	204	13.77	
38	244	15.05	244	16.23	18.10	240	15.29	
39	250	15.12	250	13.97	17.09		16.49	

the relation,

$$g_c^{TTh}(\varepsilon_c) = g_{cn}^{Th}(\varepsilon_{cn}) + g_{cp}^{Th}(\varepsilon_{cp}), \tag{24a}$$

where

$$\varepsilon_{cn} = \epsilon + |V_0| \quad \text{and} \quad \varepsilon_{cp} = \varepsilon_{cn} - |V_c|, \tag{24b}$$

where ϵ is the excitation energy of neutrons from zero level. The symbol ϵ in Eq. (24b) is the same as used in Eqs. (14)–(16). Then, ε_{cn} is the neutron-excitation energy of the single-particle level density from the base of square-well potential V_0, and similarly, ε_{cp} is the proton excitation energy of the single-particle level density from a base that is higher than the base of square well V_0 by V_c. Then, ε_c is the excitation energy of the total effective single-particle level density for the composite system.

We have carried out calculations for the single-particle level density at the excitation energies that correspond to ϵ_f (Fermi energy), $\epsilon = 0, \epsilon = 14.8, 30, 50$, and 80 MeV for $V_0^i = 45$ MeV (Table VI), whereas, for $\epsilon = 14.8$ MeV, calculations also were carried out for $V_0^i = 40$ and 54 MeV (Table IV).

As discussed earlier, Eqs. (14) and (15) have been used for calculating the values of $g_{cn}^{Th}(\varepsilon_{cn})$ and $g_{cp}^{Th}(\varepsilon_{ep})$ for neutron excitation energy and proton excitation energy, respectively,

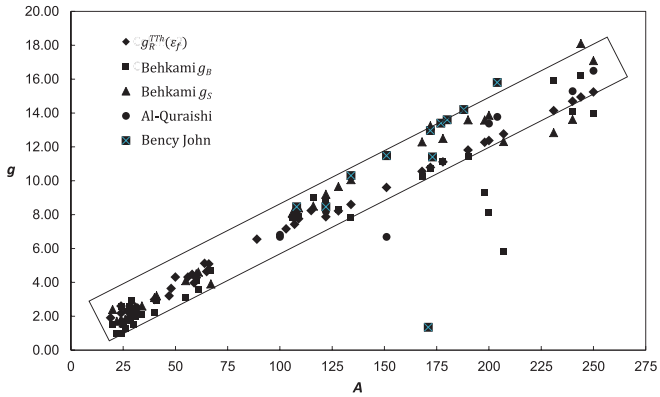

FIG. 2. (Color online) The values of $g_R^{TTh}(\varepsilon_f)$ at $V_0^i = 45$ MeV and comparison with the values calculated by Behkami *et al*. by using Bethe's model (g_B), the BCS model (g_s), and g from other authors as a function of the atomic number A (Table III).

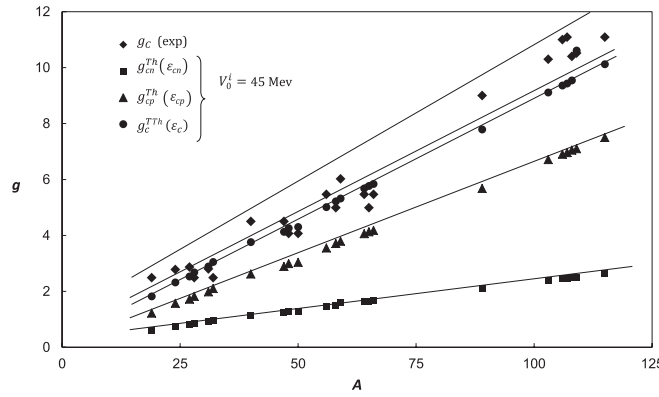

FIG. 3. The value of $g_{cp}^{Th}(\varepsilon_p)$, $g_{cn}^{Th}(\varepsilon_n)$, and $g_c^{TTh}(\varepsilon_c) = g_{cp}^{Th}(\varepsilon_{cp}) + g_{cn}^{Th}(\varepsilon_{cn})$ at $\epsilon = 14.8$ MeV and their comparison with g_c(exp) as a function of mass number A at $V_0^i = 45$ MeV (Table IV).

so that, for neutron excitation energy,

$$g_{Cn}^{Th}(\varepsilon_{cn}) = g_{cn}^{Th}(\varepsilon_{cn}) = g_{cn}^{\mathrm{TF}}(\varepsilon_{cn}) - g_{cn}^{\mathrm{free}}(\varepsilon_{cn}). \qquad (25)$$

Operationally, for neutron excitation energy ε_{cn}, the term $(\epsilon - V_0)^{1/2}$ in Eq. (14) is replaced by $(\varepsilon_{cn})^{1/2} = (\epsilon_n + |V_0|)^{1/2}$, and ϵ in Eq. (15) for g_{cn}(free) is replaced by ϵ_n.

On the other hand, for proton excitation energy, we write for $g_{cp}^{Th}(\varepsilon_{cp})$,

$$g_{cp}^{Th}(\varepsilon_{cp}) = g_{cp}^{\mathrm{TF}}(\varepsilon_{cp}) - g_{cp}^{\mathrm{free}}(\varepsilon_{cp}), \qquad (26)$$

where the operational term $(\epsilon - V_0)^{1/2}$ in Eq. (14) is replaced by $(\varepsilon_{cp})^{1/2} = [\epsilon_n + |V_0| - |V_c|]^{1/2}$ and ϵ_p in Eq. (15) for $g_{cp}^{\mathrm{free}}(\varepsilon_p)$ is replaced by $[\varepsilon_n - |V_c|]$. In Fig. 3, we have plotted the values of $g_{cn}^{Th}(\varepsilon_{cn})$, $g_{cp}^{Th}(\varepsilon_{cp})$, and $g_C^{TTh}(\varepsilon_c) = g_c^{TTh}(\varepsilon_c) =$

TABLE IV. Theoretical values of single-particle level densities $g_{cn}^{Th}(\varepsilon_{cn})$ for the excitation of neutrons, $g_{cp}^{Th}(\varepsilon_{cp})$ for the excitation of protons, and $g_c^{TTh}(\varepsilon_c)$ for the total for the (n,p) reaction, which use the 14.8 incident energy of neutrons as the excitation energy so that $g_c^{TTh}(\varepsilon_c) = g_{cn}^{Th}(\varepsilon_{cn}) + g_{cp}^{Th}(\varepsilon_{cp})$ for $V_0^i = 54$, 45, and 40 MeV based on Shlomo's model $\varepsilon_n = \epsilon_{\mathrm{inc}} + |V_0|$ and $\varepsilon_p = \varepsilon_n - |V_c|$. Also given are the experimental values of g_c(exp).

S. number	A	g_c(exp)	$V_0^i = 54$ MeV			$V_0^i = 45$ MeV			$V_0^i = 40$ MeV		
			$g_{cn}^{Th}(\varepsilon_{cn})$	$g_{cp}^{Th}(\varepsilon_{cp})$	$g_c^{TTh}(\varepsilon_c)$	$g_{cn}^{Th}(\varepsilon_{cn})$	$g_{cp}^{Th}(\varepsilon_{cp})$	$g_c^{TTh}(\varepsilon_c)$	$g_{cn}^{Th}(\varepsilon_{cn})$	$g_{cp}^{Th}(\varepsilon_{cp})$	$g_c^{TTh}(\varepsilon_c)$
1	19	2.49	0.71	1.24	1.95	0.61	1.22	1.82	0.54	1.23	1.77
2	24	2.78	0.87	1.57	2.44	0.75	1.57	2.32	0.68	1.60	2.28
3	27	2.87	0.94	1.73	2.67	0.81	1.72	2.53	0.73	1.75	2.48
4	28	2.49	0.99	1.82	2.81	0.85	1.82	2.68	0.77	1.87	2.64
5	31	2.80	1.06	1.98	3.04	0.91	1.98	2.89	0.82	2.02	2.84
6	32	2.49	1.10	2.07	3.17	0.95	2.10	3.05	0.86	2.14	3.00
7	40	4.50	1.33	2.59	3.92	1.14	2.62	3.76	1.04	2.69	3.73
8	47	4.50	1.44	1.86	4.30	1.24	2.89	4.13	1.12	2.98	4.11
9	48	4.07	1.48	3.00	4.48	1.27	2.99	4.26	1.14	3.03	4.18
10	50	4.07	1.51	3.07	4.58	1.28	3.04	4.30	1.15	3.08	4.23
11	56	5.47	1.70	3.54	5.24	1.46	3.55	5.01	1.31	3.62	4.93
12	58	6.02	1.77	3.71	5.48	1.51	3.71	5.22	1.36	3.78	5.14
13	59	4.99	1.79	3.75	5.54	1.59	3.79	5.32	1.39	3.89	5.28
14	64	4.99	1.90	4.06	5.96	1.62	4.06	5.68	1.46	4.12	5.57
15	65	5.47	1.92	4.10	6.02	1.64	4.13	5.77	1.49	4.22	5.71
16	66	5.47	1.94	4.17	6.11	1.66	4.18	5.84	1.49	4.25	5.75
17	89	9.00	2.48	5.67	8.05	2.11	5.68	7.79	1.90	5.77	6.67
18	103	10.30	2.82	6.69	8.91	2.40	6.71	9.11	2.16	6.83	8.99
19	106	11.00	2.89	6.89	9.78	2.46	6.90	9.36	2.21	7.02	9.23
20	107	11.09	2.91	6.96	9.87	2.47	6.96	9.43	2.22	7.06	9.28
21	108	10.40	2.93	7.02	9.95	2.49	7.05	9.54	2.24	7.18	9.43
22	109	10.52	2.95	7.09	10.04	2.51	7.10	10.61	2.25	7.22	9.48
23	115	11.09	3.08	7.50	10.58	2.62	7.50	10.12	2.35	7.62	9.97

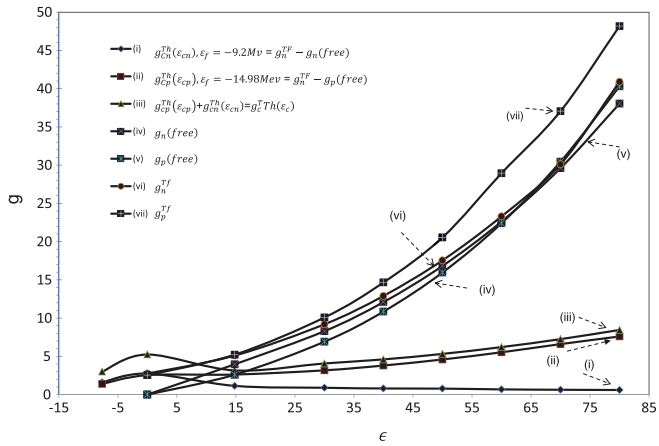

FIG. 4. (Color online) The values $g^{Th}_n(\varepsilon_{cn})$, $g^{Th}_p(\varepsilon_{cp})$, $g^{Th}_c(\varepsilon_c) = g^{Th}_{np}(\varepsilon_{cp}) + g^{Th}_{cn}(\varepsilon_{cn})$, $g^{\rm TF}_p$, $g^{\rm TF}_n$, g_p(free), and g_n(free) versus the excitation energy ϵ from negative energy ϵ_f(Fermi) up to $\epsilon = 80$ MeV for ^{40}Ca as the target.

$g^{Th}_{cn}(\varepsilon_{cn}) + g^{Th}_{cp}(\varepsilon_{cn})$ as a function of A for $V^i_0 = 45$ MeV along with g_c(exp) for $\epsilon_n = 14.8$ MeV. It is obvious that points that correspond to g_c(exp) are, in general, higher than the corresponding values of $g^{TTh}_c(\varepsilon_c)$. The calculations at $\epsilon_n = 14.8$ MeV served as a test case for the energy dependence of the single-particle level density for excitation to positive energies that correspond to the composite system. It led to the calculations for $g^{TTh}_{cn}(\varepsilon_c)$ at other energies ϵ to finally arrive at the correct value of (ε_c) for which $g_{c\langle\exp\rangle}$ is equal to $g^{TTh}_c(\varepsilon_c)$.

C. Physical interpretation

To get an insight into the general trends of the values of g's from theoretical calculations, we have plotted in Fig. 4 and given in Table V, the theoretical contributions to the overall curve of $g^{TTh}_c(\varepsilon_c)$ versus excitation energies of ϵ *at* ϵ_{Fermi}, $\epsilon = 0, \epsilon = 14.8, 30, 50$, and 80 MeV for, ^{40}Ca with $V^i_0 = 45$ MeV. We have plotted in the figure the value of $g^{Th}_{cn}(\varepsilon_{cn})$, $g^{Th}_{cp}(\varepsilon_{cp})$, $g^{Th}_{cn}(\varepsilon_{cn}) + g^{Th}_{cp}(\varepsilon_{cp}) = g^{TTh}_c(\varepsilon_c)$, $g_n$free$(\varepsilon > 0)$, $g_p$free $(\epsilon > 0)$, $g^{TF}_n(\varepsilon_{cn})$, and $g^{Th}_{cp}(\varepsilon_{cp})$ as a function of ϵ. We find that $g^{Th}_{cn}(\varepsilon_{cn})$, $g^{Th}_{cp}(\varepsilon_{cp})$, and $g^{Th}_{cn}(\varepsilon_{cn}) + g^{TTh}_{cp}(\varepsilon_{cp}) = g^{TTh}_c(\varepsilon_c)$ have peaks at $\epsilon = 0$; but whereas, $g_{cn}(\varepsilon_{cn})$ goes down at higher energies beyond 14.8 MeV, the values of $g_{cp}(\varepsilon_{cp})$ slowly go up. This difference in behavior of $g^{Th}_{cp}(\varepsilon_{cp})$ and $g^{TTh}_{cn}(\varepsilon_{cn})$ arises due to Coulomb effects on g_p(free) and $g^{\rm TF}_p(\varepsilon_{cp})$. Such general trends are evident for all the cases discussed in our paper. However, these trends do not affect our results as we have considered only $g^{Th}_{cn}(\varepsilon_{cn}) + g^{Th}_{cp}(\varepsilon_{cp}) = g^{TTh}_c(\varepsilon_c)$. As, for example, the value of $g_c(\exp) = 4.5$ is explained only by $g^{TTh}_c(\varepsilon_c)$ for neutron-plus-proton excitation. Our effective experimental values of g_c(exp) lie at ϵ between 0 and 14.8 MeV excitation as expected on the basic physical picture of a few steps that involve $(h \leqslant 2)$ in the preequilibrium process in the reactions, such as (n,p,γ), (n,np,γ), or (n,p,n,γ), which are expected to contribute to proton spectra in experimental data.

In Fig. 5, we have plotted the values of $g^{TTh}_c(\varepsilon_c)$ by using Eq. (24a) as a function of ϵ where, as mentioned earlier, we specifically have calculated $g^{TTh}_c(\varepsilon_c)$ for the Fermi energy ϵ_f and for $\epsilon = 0$, 14.8, 30, 50, and 80 MeV for $V^i_0 = 45$ MeV (Table VI). We also have indicated the values of g_R(exp) at the Fermi energy and g_c(exp) at $\epsilon = 14.8$ MeV. It is interesting to note that, as previously described, the values of g_R(exp) agree reasonably well with the values of $g^{TTh}_c(\varepsilon_f)$ obtained from Shlomo's model with $V^0_i = 45$ MeV at the Fermi energy. But the values of g_c(exp) are, in general, higher than $g^{TTh}_c(\varepsilon_c)$ for $\epsilon = 14.8$ MeV lower than expected at $\epsilon = 0$.

From Shlomo's model, it is possible to get the exact value of excitation energy ε_c that corresponds to g_c(exp) by interpolation between the values of $g^{TTh}_c(\epsilon_c)$ at $\epsilon = 0$ to $\epsilon = 14.8$ MeV (Fig. 5). It will be given by

$$\epsilon_c = \frac{14.8}{g^{TTh}_c(\epsilon = 0\ \text{MeV}) - g^{TTh}_c(\epsilon = 14.8\ \text{MeV})} \times \left[g^{TTh}_c(\epsilon = 0\ \text{MeV}) - g_c(\exp)\right]. \quad (27a)$$

Then,

$$\varepsilon_c = V_0 + \epsilon_c, \quad (27b)$$

whereas, for neutron excitation, $V^n_0 = V_{0n}$ [Eq. (17)] with $t_3 = 1$ with $V^i_0 = 45$ MeV so that $\varepsilon_{cn} = V^n_0 + \epsilon_c$ but for proton excitation $V^p_0 = V_{0p} - V_c$ with $V^i_0 = 45$ MeV so that

TABLE V. The values of $g^{Th}_{cn}(\varepsilon_{cn})$, $g^{Th}_{cp}(\varepsilon_{cp})$, $g^{TTh}_c(\varepsilon_c) = g^{Th}_{cn}(\varepsilon_{cp}) + g^{Th}_{cn}(\varepsilon_{cn})$, g_p(free), g_n(free)$g^{\rm TF}_n$, and $g^{\rm TF}_p$ for $^{40}_{20}$Ca at different excitation energies.

	For ϵ_f	$\epsilon = 0$ MeV	$\epsilon = 14.8$ MeV	$\epsilon = 30$ MeV	$\epsilon = 40$ MeV	$\epsilon = 50$ MeV	$\epsilon = 60$ MeV	$\epsilon = 70$ MeV	$\epsilon = 80$ MeV
$g^{Th}_{cn}(\varepsilon_{cn})$	1.6	2.75	1.14	0.89	0.80	0.78	0.68	0.63	0.60
$g^{Th}_{cp}(\varepsilon_{cp})$	1.39	2.54	2.62	3.17	3.8	4.59	5.53	6.6	7.6
$g^{Th}_{cp}(\varepsilon_{cp}) + g^{Th}_{cn}(\varepsilon_{cn}) = g^{Th}_c(\varepsilon_c)$	3.0	5.29	3.16	4.07	4.60	5.32	6.21	7.25	8.45
g_n(free)	0	0	3.96	8.29	12.09	16.82	22.62	29.6	38.04
g_p(free)	0	0	2.60	6.91	10.85	15.96	22.4	30.45	40.30
g^{TF}_n	1.6	2.75	5.10	9.19	12.90	17.55	23.30	30.1	40.90
g^{TF}_p	1.39	2.54	5.22	10.08	14.66	20.54	28.94	37.05	48.18

$g_R(\exp) = 2.98$, $g_c(\exp) = 4.5$, $\varepsilon_c = 47.30$ MeV, $\epsilon_c = 5.5$ MeV

$\varepsilon_c = \frac{1}{2}[(45.0 + 5.50) + (45.0 - 6.39 + 5.5)] = 47.30$ MeV

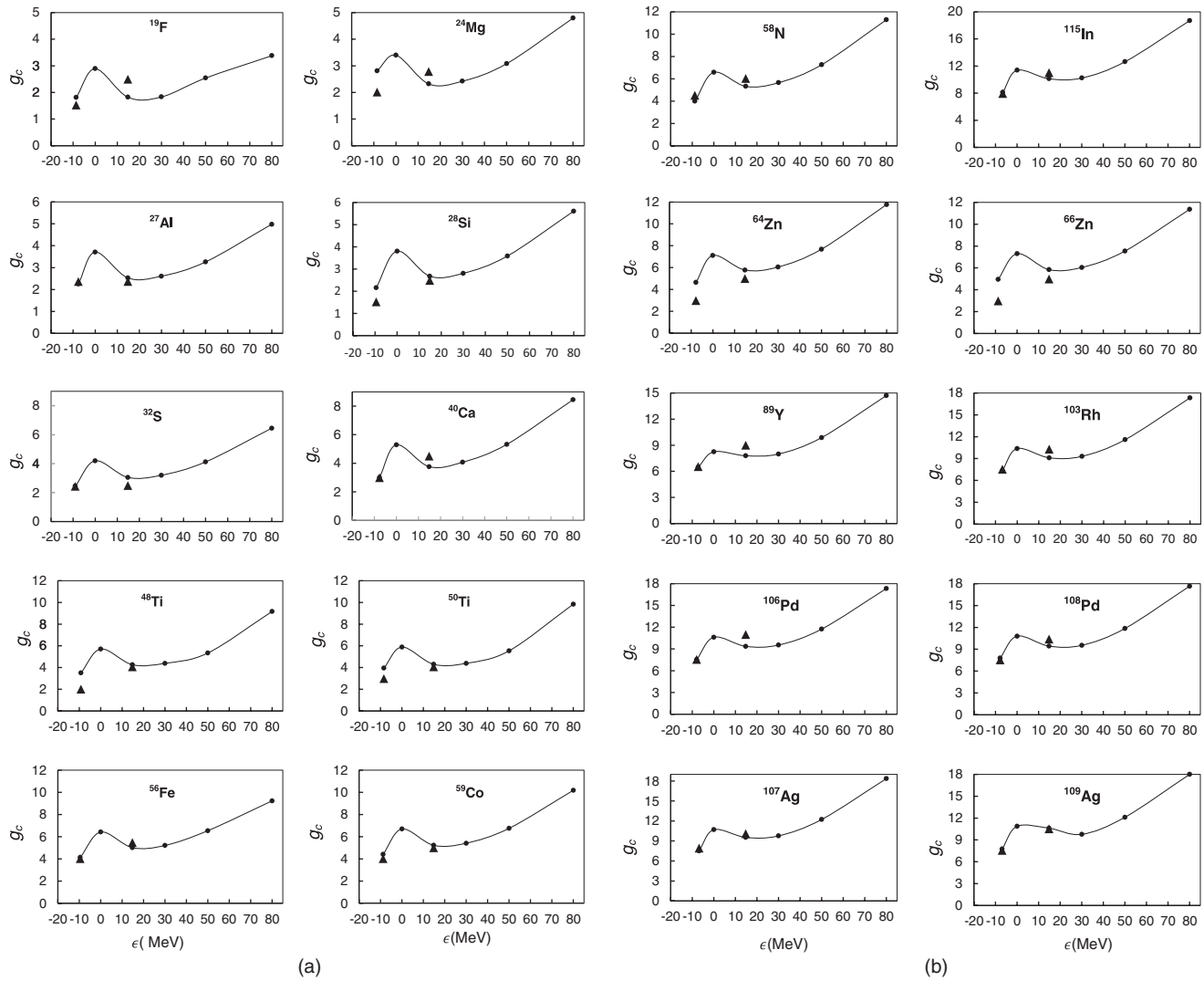

FIG. 5. The value of $g_c^{TTh}(\varepsilon_{cn})$ as a function of excitation energy ϵ from negative values of ϵ up to values of $\epsilon = 80$ MeV calculated by using Shlomo's model, which include the values of $g_c^{TTh}(\varepsilon_f)$ at Fermi energy along with g_c(exp) at $\epsilon \simeq 14.8$ MeV and g_R(exp) at the Fermi energy (Table I).

$\varepsilon_{cp} = V_0^p + \epsilon_c$. V_{0p} is given by Eq. (17), which uses $t_3 = -1$. Then,

$$\langle \varepsilon_c \rangle = \frac{\varepsilon_{cn} + \varepsilon_{cp}}{2} = \frac{V_0^n + V_0^p}{2} + \epsilon_c = \langle V_0 \rangle + \epsilon_c. \qquad (27c)$$

We have assumed that $g_c^{TTh}(\epsilon_c)$ decreases from $\epsilon = 0$ to $\epsilon = 14.8$ MeV linearly, which only is approximately correct.

As evident from Fig. 5, we also found that the experimental values of single-particle densities g_c(exp) involved in the excitation in the composite system not only match with the expected theoretical values of $g_c^{TTh}\langle \varepsilon_c \rangle$ that correspond to positive values of ϵ_c, but also match with negative values of ϵ_B below the zero-ground energy. We have calculated $\langle \varepsilon_B \rangle$ from the relation,

$$\langle \varepsilon_B \rangle = \frac{V_0^n + V_0^p}{2} - \epsilon_B, \qquad (27d)$$

where ϵ_B denotes the energy below ground energy by matching the experimental values of g_c(exp) with $g_c^{TTh}(\epsilon)$ for $\epsilon = -\epsilon_B$.

In Table VII, we have summarized the values of ϵ_c, ε_{cn}, and ε_{cp} and $\langle \varepsilon_c \rangle$, ϵ_B, and $\langle \varepsilon_B \rangle$ as calculated from Eqs. (27a)–(27d) and the values of V_0^n, V_0^p, $\langle V_0 \rangle = (V_v^n + V_0^p)/2$, V_0^p, $\langle V_0 \rangle = (V_0^n + V_0^p)/2$, and V_c. In calculating the values of ϵ_c, we have taken the values of $g_c^{TTh}(\epsilon = 0$ MeV) and $g_c^{TTh}(\epsilon = 14.8$ MeV) from Table VI, whereas, the values of g_c(exp) used in Eq. (27a) are taken from Table I. In Eq. (27c), the values of V_c are given in Table VII.

The values of $\langle \varepsilon_c \rangle$ and $\langle \varepsilon_B \rangle$ correspond to the same value of single-particle level density g_c(exp). However, $\langle \varepsilon_c \rangle$ corresponds to single-particle level density for unbound states and may be interpreted more appropriately as being involved in the MSD contribution to the preequilibrium process, which is observed experimentally.

Similarly, g_c(exp), which corresponds to $\langle \varepsilon_B \rangle$, may be interpreted as a single-particle level density for bound single-particle states that represent the MSC process. It seems that the effect of single-particle level density increases successively from the Fermi energy $\langle \varepsilon_f \rangle$ to the bound state at $\langle \varepsilon_B \rangle$ and then

TABLE VI. Theoretical values of total single-particle level densities $g_c^{TTh}(\varepsilon_f)$ based on Shlomo's model for $V_0^i = 45$ MeV for ϵ_f (for the Fermi energy) and excitation energies [Eq. (24a)] where $\epsilon_i = 0$, 14.8, 30, 50, and 80 MeV for $V_0^i = 45$ MeV. The value of ϵ_f is taken as $\epsilon_f = \frac{V_0^n + V_0^p}{2} - \varepsilon_f$. The values of $\frac{V_0^n + V_0^p}{2}$ are taken from Table VII, and ε_f is taken from Table II.

S. number	Target	ϵ_f (Negative)	$g_R^{TTh}(\varepsilon_f)$ for ε_f	$g_c^{TTh}(\varepsilon_0)$ $\epsilon_0 = 0$ MeV	$g_c^{TTh}(\varepsilon_1)$ $\epsilon_1 = 14.8$ MeV	$g_c^{TTh}(\varepsilon_2)$ $\epsilon_2 = 30$ MeV	$g_c^{TTh}(\varepsilon_3)$ $\epsilon_3 = 50$ MeV	$g_c^{TTh}(\varepsilon_4)$ $\epsilon_4 = 80$ MeV
1	^{19}F	8.61	1.81	2.89	1.82	1.83	2.54	3.38
2	^{24}Mg	8.54	2.04	3.40	2.32	2.42	3.08	4.79
3	^{27}Al	7.58	2.26	3.71	2.53	2.61	3.26	4.98
4	^{28}Sc	9.45	2.16	3.81	2.68	2.81	3.59	5.61
5	^{31}P	7.66	2.51	4.10	2.89	2.99	3.77	5.79
6	^{32}S	9.02	2.45	4.20	3.05	3.20	4.12	6.45
7	^{40}Ca	7.66	3.00	5.29	3.76	4.07	5.32	8.45
8	^{47}Ti	7.38	3.18	5.32	4.13	4.42	5.75	9.01
9	^{48}Ti	9.21	3.51	5.71	4.26	4.39	5.34	9.17
10	^{50}Ti	8.42	3.95	5.89	4.30	4.39	5.54	9.84
11	^{56}Fe	9.57	4.13	6.42	5.01	5.21	6.54	9.23
12	^{59}Co	8.88	4.41	6.69	5.22	5.41	6.75	10.18
13	^{58}Ni	8.75	3.99	6.58	5.32	5.65	7.26	11.29
14	^{65}Cu	7.22	5.03	7.22	5.68	5.82	7.20	10.72
15	^{64}Zn	7.80	4.64	7.11	5.77	6.05	7.68	11.77
16	^{66}Zn	8.88	4.95	7.30	5.84	6.04	7.54	11.36
17	^{89}Y	7.23	6.48	8.25	7.79	7.99	9.88	14.71
18	^{103}Rh	6.84	7.36	10.38	9.11	9.31	11.60	17.33
19	^{106}Pd	7.94	7.54	10.62	9.36	9.54	11.74	17.33
20	^{108}Pd	7.89	7.78	10.80	9.43	9.54	11.85	17.66
21	^{107}Ag	6.83	7.52	10.70	9.54	9.77	12.23	18.36
22	^{109}Ag	6.94	7.75	10.87	10.61	9.77	12.11	18.00
23	^{115}In	6.64	8.10	11.38	10.12	10.23	12.63	18.69

to the unbound state $\langle \varepsilon_c \rangle$ with the excitation energy as the reaction process develops from compound nucleus to MSC and finally to the MSD process.

As we plotted $\langle \varepsilon_c \rangle$, $\langle \varepsilon_B \rangle$, and $\langle \varepsilon_f \rangle$ versus mass number A of the target nuclei, interesting structure effects appear as described below.

As discussed earlier, we have derived the values of excitation energies $\langle \varepsilon_c \rangle$ of the composite system by comparing g_c(exp) derived from the Kalbach model (in relation to experimental data) with $g_c^{TTh}(\varepsilon_c)$ derived from Shlomo's model. It is extremely interesting to observe from Fig. 7, where we have plotted the values of $\langle \varepsilon_c \rangle$ as a function of A; that the excitation energies have a structure as a function of A that is related to nuclear shell structure. The values of excitation energies $\langle \varepsilon_c \rangle$ are low for nuclei that have $(Z,A) = (8,20)$, $(20,40)$, and $(28,58)$, which not only have magic proton numbers, but also have even numbers of neutrons. The nucleus with $(Z,A) = (39,89)$, i.e., ^{89}Y, has an odd number of protons but a magic number of neutrons ($N = 50$). On the other hand, nuclei, which lie at nonmagic numbers $(Z,A) = (14,28)$, $(22,48)$, and $(30,66)$ have high values of $\langle \varepsilon_c \rangle$.

Higher values of V_c for higher A and Z (from $A = 89$ to $A = 115$) yield lower values of $\langle \varepsilon_c \rangle$ as shown in Fig. 7.

It is interesting that the values of $\langle \varepsilon_B \rangle$, when plotted against A (Fig. 8), also seem to show shell structure but with higher

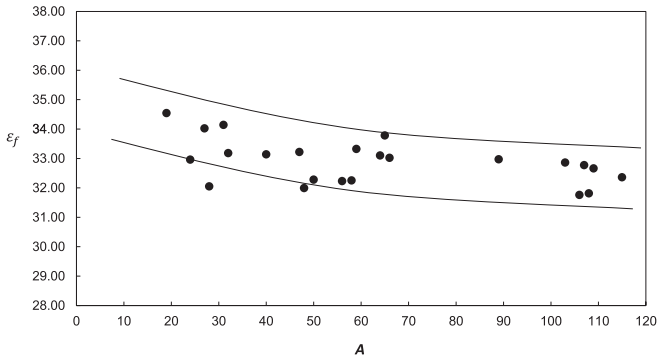

FIG. 6. The values of $\langle \varepsilon_c \rangle$ as a function of A.

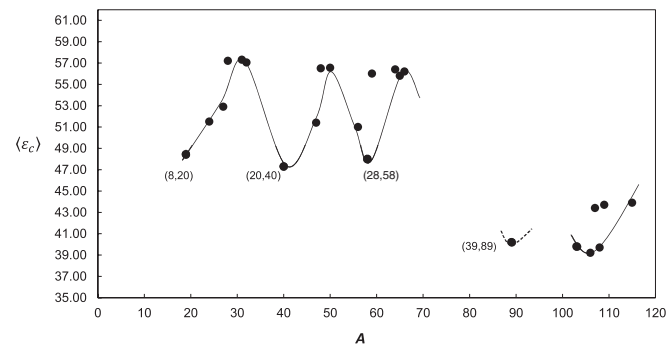

FIG. 7. The values of $\langle \varepsilon_B \rangle$ as a function of A.

TABLE VII. The values of ϵ_c, V_0^n, ε_{cn}, $(V_0^p = V_p - V_c)$, ε_{cp}, $\langle V_0\rangle = \frac{V_0^n+V_0^p}{2}$, $\langle\varepsilon_c\rangle$, V_c, ϵ_B, and ε_B in MeV as obtained from Shlomo's model as derived from Eqs. (27a)–(27d) for different target nuclei. Also, see the text that contains these equations.

Number	Nucleus (Z,A)	ϵ_c	$V_0^n = V_{0n}$	$\varepsilon_{cn} = V_0^n + \epsilon_c$	$V_0^p = V_{0p} - V_c$	$\varepsilon_{cp} = V_0^p + \epsilon_c$	$\frac{V_0^n+V_0^p}{2} = \langle V_0\rangle$	$\langle\varepsilon_c\rangle$	V_c	ϵ_B (Negative)	ε_B
1	^{19}F	5.44	43.3	48.74	43.0	48.4	43.15	48.6	3.68	3.0	40.15
2	^{24}Mg	8.3	45	53.3	41.5	49.8	43.3	51.6	4.54	6.7	36.6
3	^{27}Al	10.3	43.8	54.1	41.5	51.2	42.6	52.9	4.73	6.06	36.6
4	^{28}Sc	14.8	45	59.8	39.96	54.7	42.5	57.3	5.04	6.6	35.9
5	^{31}P	14.8	43.09	58.9	40.83	55.8	42.8	57.6	5.22	5.7	37.1
6	^{32}S	14.8	45.0	59.8	39.5	54.3	42.2	57.05	5.50	6.5	35.7
7	^{40}Ca	5.5	45	50.5	38.6	44.1	41.8	47.3	6.39	3.4	37.4
8	^{47}Ti	8.8	42.9	51.7	40.3	51.1	41.6	50.4	6.81	3.3	37.3
9	^{48}Ti	14.8	42.3	57.1	41.10	55.9	41.2	56.0	6.61	5.9	35.3
10	^{50}Ti	14.8	41.0	55.8	42.53	57.3	41.7	56.50	6.52	6.1	35.6
11	^{56}Fe	9.2	43.9	53.1	39.7	48.88	41.8	51.0	7.42	5.0	36.8
12	^{59}Co	14.8	42.3	57.5	40.1	53.0	41.2	56.0	7.58	6.5	34.7
13	^{58}Ni	6.5	43.9	48.8	38.2	46.62	41.0	47.50	7.90	2.6	38.4
14	^{65}Cu	14.8	41.0	55.8	41.1	55.01	41.0	55.8	7.88	5.4	35.6
15	^{64}Zn	14.8	45	59.8	36.68	53.0	40.9	55.7	8.19	4.8	36.6
16	^{66}Zn	14.8	45	56.8	40.09	55.69	42.9	57.7	8.11	6.2	35.7
17	^{89}Y	0	41.0	41.0	39.5	39.46	40.2	40.2	9.54	0.0	40.2
18	^{103}Rh	09	41.0	41.1	38.5	39.60	39.7	39.8	10.19	1.58	38.1
19	^{106}Pd	0	40.5	40.5	38.5	38.98	39.7	39.7	10.52	0.0	39.7
20	^{108}Pd	0	41.0	41.0	38.2	38.45	39.7	39.7	10.55	2.4	37.3
21	^{107}Ag	3.8	41.0	44.8	39.3	41.98	39.6	43.4	10.82	2.3	37.3
22	^{109}Ag	4.06	41.0	45.06	38.5	42.31	39.6	43.7	10.75	2.6	37.0
23	^{115}In	4.4	41.0	45.4	38.2	42.40	39.0	43.4	11.01	3.3	35.7

values at magic members and lower values at nonmagic numbers. This is opposite to the behavior of shell structure for $\langle\varepsilon_c\rangle$. On the other hand, when the values of $\langle\varepsilon_f\rangle$ are plotted against A, as in Fig. 6, there is no strong indication of any shell structure.

Furthermore, we have calculated the values of $f(\text{exp})$ in the relation,

$$28\frac{g_c(\text{exp})}{g_R(\text{exp})} = \left[\frac{\langle\varepsilon_c\rangle}{\langle\varepsilon_f\rangle}\right]^{1/2} f(\text{exp}), \tag{28a}$$

and we have tabulated the same in Table VIII. The average value of $f(\text{exp})$ for all targets comes out to be 1.2 ± 0.2. In Fig. 9, the values of $f(\text{exp})$ are plotted as a function of A. The value of ε_c is greater than $\langle\varepsilon_f\rangle$ and corresponds to ϵ_c between $\epsilon_c = 0$ and 14.8. Also, we have calculated the values of $f(\text{Theor})$ from the relationship,

$$\frac{g_c^{TTh}(\varepsilon_c)}{g_R^{TTh}(\varepsilon_f)} = \left[\frac{\langle\varepsilon_c\rangle}{\langle\varepsilon_f\rangle}\right]^{1/2} f(\text{Theor}) \tag{28b}$$

for values of $\epsilon_c = 0, 2, 5, 10, 14.8, 20, 25, 30, 40, 50$, and 60 MeV for three targets (i) ^{40}Ca, (ii) ^{64}Zn, and (iii) ^{115}In.

It seems that the value of $f(\text{Theor})$ is nearly 1 for $\epsilon = 15$ to $\epsilon = 60$ MeV. For $\epsilon \leqslant 15$, the values of $f(\text{Theor})$ are higher and extend up to $f(\text{Theor}) \cong 1.3 - 1.4$ for $\epsilon = 0$. The average $f(\text{exp})$ for all targets comes out to be

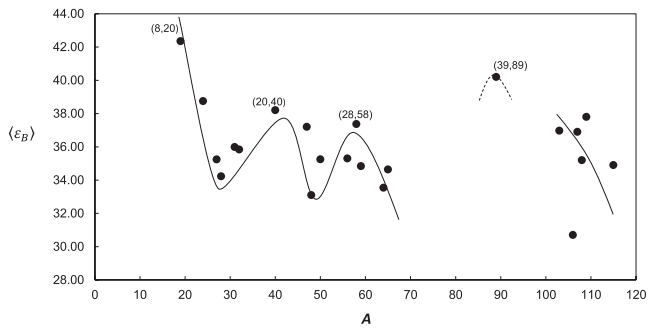

FIG. 8. The values of $\langle\varepsilon_f\rangle$ plotted against A of the target for $V_0^i = 45$ MeV.

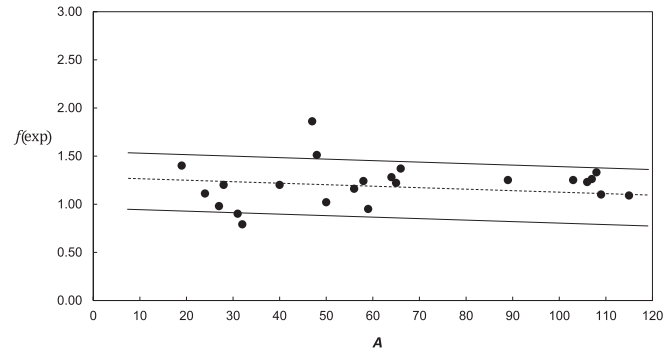

FIG. 9. The values of $f(\text{exp})$ in the relationship of $\frac{g_c(\text{exp})}{g_R(\text{exp})} = [\frac{\langle\varepsilon_c\rangle}{\langle\varepsilon_f\rangle}]^{1/2} f(\text{exp})$ as a function of A.

TABLE VIII. Values of $\frac{g_c(\text{exp})}{g_f(\text{exp})} = (\frac{\langle\varepsilon_c\rangle}{\langle\varepsilon_f\rangle})^{1/2} f(\text{exp})$. (b) Values of $\frac{g_c(\text{exp})}{g_f(\text{exp})} = (\frac{\langle\varepsilon_c\rangle}{\langle\varepsilon_f\rangle})^{1/2} f(\text{exp})$ for $\epsilon = 0$, 2, 5, 10, 14.8, 20, 25, 30, 40, 50, 60, 70, and 80 MeV, $g_c^{TTh}(\varepsilon_c)/g_c^{TTh}(\varepsilon_f) = (\langle\varepsilon_c\rangle/\varepsilon_f)^{1/2} f(\text{Theor})$.

S. number	Target	$\frac{g_c(\text{exp})}{g_f(\text{exp})}$	$[\langle\varepsilon_c\rangle/\langle\varepsilon_f\rangle]^{1/2}$	$f(\text{exp})$
		(a)		
1	^{19}F	1.64	1.17	1.40
2	^{24}Mg	1.38	1.23	1.11
3	^{27}Al	1.22	1.24	0.98
4	^{28}Sc	1.62	1.34	1.20
5	^{31}P	1.13	1.30	0.90
6	^{32}S	1.03	1.30	0.79
7	^{40}Ca	1.47	1.2	1.20
8	^{47}Ti	2.24	1.24	1.86
9	^{48}Ti	2.01	1.33	1.51
10	^{50}Ti	1.36	1.33	1.02
11	^{56}Fe	1.46	1.26	1.16
12	^{59}Co	1.24	1.3	0.95
13	^{58}Ni	1.5	1.21	1.24
14	^{65}Cu	1.66	1.28	1.22
15	^{64}Zn	1.68	1.3	1.28
16	^{66}Zn	1.8	1.3	1.37
17	^{89}Y	1.37	1.1	1.25
18	^{103}Rh	1.37	1.1	1.25
19	^{106}Pd	1.38	1.11	1.23
20	^{108}Pd	1.47	1.12	1.33
21	^{107}Ag	1.34	1.15	1.26
22	^{109}Ag	1.39	1.26	1.10
23	^{115}In	1.38	1.26	1.09

(b)

(1) ^{40}Ca:$g_R^{TTh}(\varepsilon_f) = 3.00$, $\langle\varepsilon_f\rangle = 33.14$ MeV; $f(\text{exp}) = 1.2$, $\epsilon_c = 5.5$ MeV.

Number	ϵ(MeV)	$g_c^{TTh}(\varepsilon_c)$	$g_c^{TTh}(\varepsilon_c)/g_R^{TTh}(\varepsilon_f)$	$\langle\varepsilon_c\rangle$	$(\langle\varepsilon_c\rangle/\langle\varepsilon_f\rangle)^{1/2}$	$f(\text{Theor})$
1	0	4.95	1.65	41.8	1.2	1.37
2	2	3.47	1.25	43.8	1.25	0.97
3	5	3.86	1.29	46.8	1.20	1.07
4	10	3.94	1.31	51.8	1.25	1.05
5	14.8	3.74	1.25	56.6	1.30	0.96
6	20	3.71	1.25	61.8	1.35	0.90
7	25	3.84	1.29	66.8	1.41	0.91
8	30	4.01	1.37	71.8	1.47	0.93
9	40	4.51	1.50	81.8	1.53	0.98
10	50	5.19	1.73	91.8	1.64	1.06
11	60	6.04	2.01	101.8	1.75	1.13
		(2) ^{64}Zn:$g_R^{TTh}(\varepsilon_f) = 4.64$, $\langle\varepsilon_f\rangle = 33.10$ MeV; $f(\text{exp}) = 1.28$, $\epsilon_c = 14.8$ MeV				
1	0	7.11	1.53	40.9	1.1	1.41
2	2	5.72	1.23	42.9	1.14	1.08
3	5	4.82	1.04	45.9	1.18	0.90
4	10	6.20	1.33	50.9	1.23	1.08
5	14.8	5.72	1.23	55.7	1.30	0.94
6	20	5.70	1.23	60.9	1.4	0.82
7	25	5.82	1.25	65.9	1.41	0.89
8	30	6.05	1.24	70.9	1.42	0.87
9	40	6.74	1.45	80.9	1.56	0.93
10	50	7.68	1.65	90.9	1.60	1.03
11	60	8.8	1.9	100.9	1.7	1.11

TABLE VIII. (*Continued.*)

(3) ^{115}In: $g_R^{TTh}(\epsilon_f) = 8.10$, $\langle\epsilon_f\rangle = 32.36$ MeV; $f(\text{exp}) = 1.09$, $\epsilon_c = 4.9$ MeV

Number	ϵ(MeV)	$g_c^{TTh}(\epsilon_c)$	$g_c^{TTh}(\epsilon_c)/g_R^{TTh}(\epsilon_f)$	$\langle\epsilon_c\rangle$	$(\langle\epsilon_c\rangle/\langle\epsilon_f\rangle)^{1/2}$	f(Theor)
1	0	11.38	1.40	39.0	1.1	1.29
2	2	10.10	1.25	41.0	1.1	1.14
3	5	6.42	0.79	44.0	1.17	0.68
4	10	10.18	1.08	49.0	1.22	0.88
5	14.8	10.10	1.24	53.8	1.30	0.95
6	20	9.81	1.21	59.0	1.18	1.03
7	25	9.92	1.22	64.0	1.4	0.87
8	30	10.23	1.26	69.0	1.07	1.18
9	40	11.23	1.38	79.0	1.47	0.93
10	50	12.63	1.6	89.0	1.56	1.02
11	60	14.35	1.77	99.0	1.9	0.93

$f(\text{exp}) \cong 1.2 \pm 0.2$ for which ϵ lies between 0 and 15 MeV. We, therefore, conclude that Shlomo's theory explains the values of $f(\text{exp})$ in the relationship given in Eq. (28a). For $\epsilon < 15$ MeV, the Coulomb effect is important, and $g(\text{free})$ for $\epsilon > 0$ plays an important part. This also explains the values of $f(\text{exp})$ for ^{40}Ca, ^{69}Zn, and ^{115}In by using Shlomo's theory.

Blann [25,26] described an experiment at 200 MeV energy of protons where authors measured the values of g_c and g_f and showed that a relationship like Eq. (28) holds well for $f = 1$, which corresponds to high values of excitation energy.

IV. SUMMARY OF RESULTS

(i) The analysis of the experimental data of the energy spectrum and angular distribution of protons in the (n,p) reaction at 14.8 MeV incident energy, as undertaken earlier [1] by using the Kalbach model, has resulted in extracting two values of single-particle level densities for many targets that lie on a smooth curve when plotted against A [1]; (i) $g_R(\text{exp})$ for the residual nuclei at the Fermi energy for bound states and (ii) $g_c(\text{exp})$for the composite system for unbound states (Table I). We found $g_c(\text{exp})$ always is greater than $g_R(\text{exp})$.

(ii) We have calculated the theoretically expected values $g_R^{TTh}(\varepsilon_f)$ by using Shlomo's model at the Fermi energy by using both neutron excitation and proton excitation processes for different values of $V_0^i = 40$, 45, 50, and 54 MeV (Table II). For proton excitation, we have used an approximate model for the Coulomb interaction. We found that the values of $g_R(\text{exp})$ almost matched exactly with $g_R^{TTh}(\varepsilon_f)$ for $V_0^i = 45$ MeV (Fig. 1). This shows that values of single-particle level density $g_R(\text{exp})$, which results from the decay after the preequilibrium emission of the composite system in the nucleus in the Kalbach model, are reproduced by Shlomo's model at the Fermi energy if we assume that excitation of both neutrons and protons is involved.

Also, as shown in Table III and Fig. 2, Shlomo's model nearly reproduces the values of single-particle level densities as derived by many authors by using different methods for the decay of compound states at the Fermi energy.

(iii) We have calculated the values of $g_c^{TTh}(\varepsilon_c)$ for $\epsilon = 14.8$ MeV excitation energy as a test case by using Shlomo's model (Table IV and Fig. 3) to compare with $g_c(\text{exp})$. It is evident that the values of $g_c(\text{exp})$ nearly are somewhat higher than $g_c^{TTh}(\varepsilon_c)$ for all nuclei.

We also calculated $g_c^{TTh}(\varepsilon_c)$ for the excitation of neutrons, protons, and the neutron plus proton for ^{40}Ca at various energies. We found that the experimental value of $g_c(\text{exp})$ gave a proper excitation energy $\langle\varepsilon_c\rangle$ if we used neutron-plus-proton excitation (Table V and Fig. 4). Hence, our assumption of neutron-plus-proton excitation for all nuclei is valid.

(iv) To obtain the exact values of $\langle\varepsilon_c\rangle$, at which $g_c(\text{exp})$ matches with $g_c^{TTh}\langle\varepsilon_c\rangle$, we have calculated the values of $g_c^{TTh}\langle\varepsilon_c\rangle$ for ϵ_f (Fermi energy), $\epsilon = 0$, 14.8, 30, 50, and 80 MeV for all the targets (Table VI and Fig. 5). By interpolation between $\epsilon = 0$ and $\epsilon = 14.8$, we could obtain the exact value of ϵ_c so that the exact value of $\langle\varepsilon_c\rangle$ could be obtained by using Eqs. (27a)–(27c). The values of ϵ_c, ε_{cn}, ε_{cp}, and $\langle\varepsilon_c\rangle$, thus, obtained are given in Table VII.

(v) In Fig. 7, we have plotted the values of $\langle\varepsilon_c\rangle$ as a function of A. It is very interesting that there is a shell structure for these values, which indicates the relationship of excitation energies with the nuclear structure. The values of the excitation energies (ε_c) for target nuclei are low at magic numbers and high at nonmagic numbers.

This supports the interpretation of interaction as required for the preequilibrium in the Kalbach model of the MSD process.

On the other hand, the values of $\langle\varepsilon_B\rangle$, which correspond to the negative values of ϵ_B as given in Table VIII and which are shown in Fig. 8, also show the shell structure, which is complementary to the shell structure that corresponds to the shell structure for $\langle\varepsilon_c\rangle$. This seems to lead to the interpretation that energies $\langle\varepsilon_B\rangle$ correspond to the MSC process.

The values of $\langle \varepsilon_f \rangle$ plotted as a function of A in Fig. 6 do not seem to give any strong indication of such a shell structure.

V. CONCLUSION

Earlier Ref. [1], we analyzed the data of the experimental values of the energy spectra and the angular distribution of protons in the (n,p) reaction in terms of the Kalbach model for the preequilibrium process to find the effective single-particle level density $g_c(\text{exp})$ for the composite system and the effective single-particle level density $g_R(\text{exp})$ for residual nuclei.

(i) We found that $g_c(\text{exp})$ always is greater than $g_R(\text{exp})$. To understand this difference, for the variation in magnitude of the single-particle level density with excitation energy, we have carried out the calculations by using Shlomo's model.

From these calculations, we conclude that, for the present excitation energy of $\langle V_0 \rangle + 14.8$ MeV of the composite system, the contribution of the MSD in the preequilibrium process becomes dominant. The excitation energies $\langle \varepsilon_c \rangle = V_0 + \varepsilon_c$, which correspond to the single-particle level density $g_c(\text{exp})$, are less than $\langle V_0 \rangle + 14.8$ MeV for many cases; but in some cases, they approach this value (Fig. 7). It is, however, always more than the Fermi energy $\langle \varepsilon_f \rangle$ as obtained from the calculations based on Shlomo's model to define $g_R(\text{exp})$ (Table II and Figs. 6 and 7).

(ii) The variation in $g_c(\varepsilon_c)$ with (ε_c) can be parametrized by Shlomo's theory as

$$g_c(\varepsilon_c) = g(\varepsilon_f)\left[\frac{\langle \varepsilon_c \rangle}{\langle \varepsilon_f \rangle}\right]^{1/2} f. \tag{28c}$$

It seems that the values of $f(\text{Theor})$ below $\langle \varepsilon_c \rangle = \langle V_0 \rangle + 15$ MeV extend up to 1.3–1.4 for$\langle \varepsilon_c \rangle = \langle V_0 \rangle$. The values of $f(\text{exp})$ for ^{40}Ca, ^{64}Zn, and ^{115}In fall in this range within the experimental error and, thus, are explained by Shlomo's theory (Fig. 10 and Table VIII). The average values of $f(\text{exp})$ for all targets turns out to be $10.2 + 0.2$ for values of $\langle \varepsilon_c \rangle$ and $\langle \varepsilon_f \rangle$, calculated on the basis of Shlomo's theory to fit the experimental values of $g_c(\text{exp})$ and $g_R(\text{exp})$ (Fig. 9 and Table VIII). This also seems to be in accord with Shlomo's theory. The values of $f(\text{Theor})$ for above $\langle \varepsilon_c \rangle = V_0 + 15$ MeV are, in general, nearly close to 1.

(iii) Excitation energies $\langle \varepsilon_c \rangle$ for single-particle level densities, when plotted versus A, exhibit strong nuclear structure effects [such as even-odd, shell, or magic number effects (Fig. 7)]. However, the values of $\langle \varepsilon_f \rangle$, when plotted against A, do not show any large tendency for these structure effects (Fig. 6).

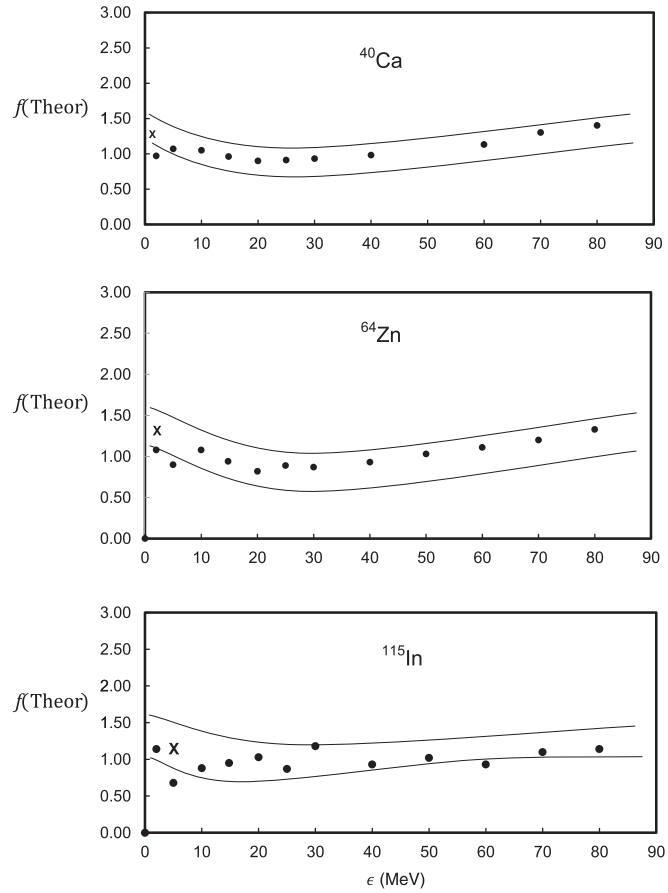

FIG. 10. The values of $f(\text{Theor})$ as a function of ϵ used in the relationship $\frac{g_c^{TTh}(\varepsilon_c)}{g^{TTh}(\varepsilon_f)} = (\frac{\langle \varepsilon_c \rangle}{\langle \varepsilon_f \rangle})^{1/2} f(\text{Theor})$ for ^{40}Ca, ^{64}Zn, and ^{115}In. The $f(\text{exp})$ for these cases are indicated by the symbol X.

(iv) The alternate values of excitation energies $\langle \varepsilon_B \rangle$ for the bound effective single-particle level density, as suggested by the theoretical calculation for the composite system, are expected to contribute to MSCs. The excitation energy $\langle \varepsilon_B \rangle$ that lies between Fermi energy $\langle \varepsilon_f \rangle$ and $\langle V_0 \rangle$ also shows nuclear structure effects when plotted against A. However, these structure effects are opposite to the structure effects for $\langle \varepsilon_c \rangle$ (Fig. 8).

ACKNOWLEDGMENT

The authors thank Professor S. Shlomo of Texas A&M University, College Station, Texas, whose comments on our draft paper helped us to finalize the present paper. We have used his theoretical model for the calculation of single-particle level densities at various excitation energies to compare with the semiempirical values based on the Kalbach model.

[1] G. Singh, H. S. Hans, T. S. Cheema, K. P. Singh, D. C. Tayal, J. Singh, and S. Ghosh, Phys. Rev. C **49**, 1066 (1994).
[2] PRECO-D2, Los Alamos National Laboratory, Los Alamos, CA, Report No. 10248-MS, 1985 (unpublished).
[3] S. Shlomo, Nucl. Phys. A **539**, 17 (1992).
[4] Y. A. Bogila, V. M. Kolomietz, A. I. Sanzahur, and S. Shlomo, Phy. Rev. C **53**, 855 (1996).
[5] S. Shlomo, V. M. Kolomietz, and H. Dejbakhsh, Phy. Rev. C **55**, 1972 (1997).
[6] S. Shlomo and G. F. Bertsch, Nucl. Phys. A **243**, 507 (1975).

[7] H. Feshbach, A. Kermann, and S. Koonin, Ann. Phys. (NY) **125**, 429 (1980).
[8] J. J. Griffin, Phys. Rev. Lett. **17**, 478 (1966); M. Blann, *ibid*. **21**, 1357 (1968).
[9] M. Blann, Phys. Rev. Lett. **27**, 337 (1976).
[10] M. Blann and H. K. Vonach, Phy. Rev. C **28**, 1475 (1983).
[11] M. Blann and A. Mignerey, Nucl. Phys. A **186**, 245 (1972).
[12] M. Blann, Phys. Rev. Lett. **28**, 757 (1972); Nucl. Phys. A **253**, 570 (1973).
[13] C. Kalbach, Z. Phys. A **283**, 401 (1977).
[14] C. Kalbach, Z. Phys. A **287**, 379 (1978).
[15] V. F. Weisskopf and D. H. Ewing, Phys. Rev. **57**, 935 (1940); **57**, 472 (1940).
[16] C. Kalbach, Phys. Rev. C **23**, 124 (1981); **25**, 3197 (1982); C. Kalbach and F. M. Mann, *ibid*. **23**, 112 (1981).
[17] V. M. Strutinsky, Nucl. Phys. A **95**, 420 (1967); **122**, 1 (1968); J. Tōke and W. J. Świątecki, *ibid*. **372**, 141 (1981).
[18] M. Brack and H. C. Pauli, Nucl. Phys. A **207**, 401 (1973).
[19] P. Ring and P. Schuck, *The Nuclear Many Body Problem* (Springer, Berlin, 1980), Chap. 13.
[20] D. L. Tubbes and S. E. Koonin, Astrophys. J. **232**, L59 (1979); D. R. Dean and U. Morsel, Z. Phys. A **322**, 647 (1985).
[21] V. S. Ramamurty, M. Asghar, and S. K. Kataria, Nucl. Phys. A **398**, 544 (1983).
[22] A. N. Behkami, Z. Kargor, and N. Nasrabedi, Phys. Rev. C **66**, 064307 (2002).
[23] S. I. Al-Quraishi, S. M. Grimes, T. N. Massey, and D. A. Resler, Phys. Rev. C **63**, 065803 (2001).
[24] Bency John, R. K. Choudhary, B. K. Nayak, A. Saxena, and D. C. Biswas, Phys. Rev. C **63**, 054301 (2001).
[25] M. Blann, Proceedings Summer School and Nuclear Physics in 1974, Pradal, Ramania Report No. 3494-13, 1975 (unpublished).
[26] M. Blann, Ann. Rev. Nucl. Sci. **25**, 123 (1975).